Journal of Neuroinflammation

RESEARCH

Open Access

CX3CR1$^+$/UCHL1$^+$ microglial extracellular vesicles in blood: a potential biomarker for multiple sclerosis

Jing Duan[1†], Aowei Lv[2†], Zhen Guo[1], Qi Liu[1], Chen Tian[1], Ying Yang[1], Jin Bi[2], Xintong Yu[2], Guoping Peng[3], Benyan Luo[3], Zhijian Cai[4], Bin Xu[1*], Ying Fu[2*] and Jing Zhang[1,5*]

Abstract

In neuroinflammation, distinguishing microglia from macrophages and identifying microglial-specific biomarkers in peripheral blood pose significant challenges. This study comprehensively profiled the extracellular vesicles (EVs) of microglia and macrophages, respectively, revealing co-expressed EVs with UCHL1 and CX3CR1 as EVs derived specifically from microglia in human blood. After extensive validation, using optimized nano flow cytometry, we evaluated plasma CX3CR1$^+$/UCHL1$^+$ EVs across clinical cohorts [multiple sclerosis (MS), HTLV-1 associated myelopathy (HAM), Alzheimer's disease (AD), and Parkinson's disease (PD)], along with established neurodegenerative markers (NMDAR2A and NFL). The findings discovered a notable rise in CX3CR1$^+$/UCHL1$^+$ EVs in MS, particularly heightened in HAM, in contrast to controls. Conversely, AD and PD exhibited unaltered or diminished levels of microglial EVs. An integrated model of CX3CR1$^+$/UCHL1$^+$, NMDAR2A$^+$, and NFL$^+$ EVs demonstrated promising diagnostic potential for distinguishing MS from controls and HAM. As to the disease duration, CX3CR1$^+$/UCHL1$^+$ EVs increased in the initial five years of MS, stabilizing thereafter, whereas NMDAR2A$^+$ and NFL$^+$ EVs remained stable initially but increased significantly in the subsequent five years, suggesting their correlation with disease duration. This study uncovers unique blood microglial EVs with potential as biomarkers for MS diagnosis, differentiation from HAM, and correlation with disease duration.

Keywords Microglia, Extracellular vesicles, Multiple sclerosis, Biomarker, UCHL1, CX3CR1

[†]Jing Duan and Aowei Lv contributed equally to this work.

*Correspondence:
Bin Xu
xubin1990@zju.edu.cn
Ying Fu
fuying1995@163.com
Jing Zhang
jzhang1989@zju.edu.cn
[1]Department of Pathology, The First Affiliated Hospital, Zhejiang University School of Medicine, Hangzhou 310003, China
[2]Department of Neurology, Institute of Neurology of First Affiliated Hospital, Fujian Medical University, Fuzhou, Fujian, China
[3]Department of Neurology, The First Affiliated Hospital, Zhejiang University School of Medicine, Hangzhou 310003, China
[4]Institute of Immunology, Department of Orthopedics of the Second Affiliated Hospital, Zhejiang University School of Medicine, Hangzhou 310009, China
[5]National Human Brain Bank for Health and Disease, Zhejiang University, Hangzhou 310012, China

Background

Significant alterations in innate and adaptive immunity have been observed in the context of aging and neurological disorders affecting the central nervous system (CNS). Key components of CNS immunity involve resident microglia and recruited peripheral macrophages, particularly in instances where the blood-brain barrier (BBB) is compromised [1, 2]. BBB damage is well-established in conditions such as stroke [3], encephalitis [4], and classical neuroinflammatory disorders like multiple sclerosis (MS) [5]. More recently, it has become evident that BBB damage and neuroinflammation are also prevalent in various neurodegenerative disorders, including HTLV-1-associated myelopathy (HAM), which resembles MS clinically [6, 7], Alzheimer's disease (AD) [8], and Parkinson's disease (PD) [9].

Assessing the activity of innate immune cells in living individuals requires a robust technique capable of quantifying and distinguishing between microglial activation and that mediated by macrophages. The most effective method currently appears to be PET studies utilizing ligands that bind to microglia, although the specificity of these ligands remains a subject of challenge [10, 11]. To circumvent this roadblock, a rapidly evolving technology is developed to focus on extracellular vesicles (EVs), which not only exhibit tissue and cell specificity but also readily traverse the BBB, facilitating the practical detection of CNS cell-specific biomarkers in peripheral blood [12].

In the last few years, blood EVs originating from neurons [13], astrocytes [14], and oligodendrocytes [15] have been documented, yet, there is currently no marker that definitively enhances the enrichment of EVs derived from CNS microglia in blood. This controversy arises primarily from the embryological similarity between microglia and macrophages. However, more recent studies have amassed compelling evidence establishing microglia as a distinct cell population separate from macrophages. Specifically, fate mapping has revealed that adult microglia originated from precursors that leave the yolk sac on E8.5–E9.0 [16, 17], whereas macrophages derived from bone marrow [18]. Moreover, microglial development is independent of the transcription factor MYB or colony-stimulating factor 1 (CSF-1) [19], both of which are essential for bone-marrow-derived macrophages [20, 21], suggesting that it is possible to identify protein markers uniquely associated with microglia.

In this investigation, we leveraged advanced proteomics technology, coupled with rigorous validation strategies, to reveal $CX3CR1^{+}$/$UCHL1^{+}$ EVs as distinctive blood biomarkers for microglia in human peripheral blood. Additionally, we showcased that the peripheral microglial biomarker, despite notable variability across diverse neurological conditions, exhibits promise for diagnosing MS and differentiating it from other diseases.

Materials and methods

The workflow to characterize microglial EVs in human blood is summarized in Supplementary Fig. S1.

Cell culture

Cell lines BV2 and RAW264.7 were cultured in DMEM (Shanghai Peiyuan, L110KJ) supplemented with 10% Fetal Bovine Serum (Gibco, 30044333), 100 μg/mL penicillin, and 100 μg/mL streptomycin (Shanghai Peiyuan, S110JV). The cells were cultured in a 5% CO_2 incubator with a humidified atmosphere of air at 37 °C.

The primary microglia were isolated from the cortex of newborn C57 mice. The brain tissue was isolated, crushed, and centrifuged at 1,000 × *g* for 5 min after removing the olfactory bulb, cerebellum, hippocampus, and meninges. Subsequently, the tissue was resuspended in 1–2 mL of 0.25% trypsin-EDTA (Shanghai Peiyuan, S310JV) for 20 s at 37 °C. An equal amount of culture medium was used to terminate the digestion. After centrifugation, the cell pellet was resuspended in F12 medium (Shanghai Peiyuan, L310KJ) supplemented with M-CSF (Absin, abs04383), filtered with a 70 μm filter, and planted on poly-D-Lysine (PDL, Sigma, P6407)-coated T75 tissue culture flasks. The culture medium was replaced by a fresh F12 medium containing M-CSF after 24 h. When the primary microglia were confluent after culturing for 10–15 days, the cells were shaken at a rotation speed of 250 rpm/min for 4–6 h. The primary microglia were subsequently collected and seeded into six-well PDL-coated plates.

The primary macrophages were isolated from the femur and tibia of 6- to 8-week-old C57 mice. After removing both ends of the bone, the bone marrow was flushed out using DMEM. The cell suspension was collected and treated with red blood cell lysis buffer for 10 min to remove erythrocytes. The cells were then centrifuged at 2,000 rpm for 10 min. After removing the supernatant, the cell pellet was washed twice with PBS. The cells were resuspended in DMEM containing 10% FBS and 10 ng/mL M-CSF and then transferred into a T75 tissue culture flask after filtering through a 70 μm disposable cell filter. The primary macrophages were used for experiments after approximately 6 days of cell culture.

Mass spectrometry

The urea (Sigma, 33247) lysis buffer (1% protease inhibitor) was used to extract the samples of EVs. The protein concentration was determined using a BCA protein assay kit (Invitrogen, 23227). SDS-PAGE (Solarbio, P1200) was used to detect the protein extraction efficiency and check for contamination. An equal amount of samples

Table 1 The list of primer sequence

Name	Forward	Reverse
Cx3cr1	GAGCATCACTGACATCTACCTCC	AGAAGGCAGTC GTGAGCTTGCA
Uchl1	GAAGCAGACCATCGGAAACTCC	GGACAGCTTCT CCGTTTCAGAC
Flt1	TGGATGAGCAGTGTGAACGGCT	GCCAAATGCAG AGGCTTGAACG
Dock4	GATAGGAGAGGTGGATGGCAAG	CGCCTTGAGATG CAGATCGTAG
Map3k5	GGTCATTCAGGCATCCGAGAAG	CAGAAGTCCAC GAGTTCCTGCT
St6gal	GCAGGATCTCTGAAGAACTCCC	TTGTGCCCACAT CCTGTTGGAAG
Hira	TCACAGAACGGTCCAAAGCCAC	CTCCTTGACGA GGTTCTGCTCT
Dgcr2	ACCACCCTATGAGGCGTCTATC	CCTTCAATGCCA CCATCTCTTGG
Entpd1	CTGGACAAGAGGAAGGTGCCTA	GACTGTCTGAGA TGAGGCTTAGC
Traf6	TTTCCCTGACGGTAAAGTGCCC	ACCTGGCACTT CTGGAAAGGAC
Dab2ip	CGAGACCCTTTCCAACACAGCA	GTGTGGACATCC CTCAGGATAC
Galnt10	CTGTGAAGCCAACGTCAACTGG	ACATTTCCCAGT CGAAGGCACC
Gapdh	CATCACTGCCACCCAGAAGACTG	ATGCCAGTGAG CTTCCCGTTCAG

was taken for analysis based on their concentration. After adding 5 mM DTT (Thermo, A39255), the samples were then incubated at 56 °C for 30 min. 11 mM IAM (Thermo, A39271) was added and the samples were further incubated at room temperature for 15 min. 100 μL of 0.1 M NH_4HCO_3 (Fisher, A643-500) was added to the ultrafiltration tube (Millipore, UFC5010) and centrifuged at 14,000 × *g* for 15 min. An appropriate amount of protein was transferred to the ultrafiltration tube and centrifuged at 14,000 × *g* for 20 min. This step was repeated three times, with the addition of 200 μL 0.1 M NH_4HCO_3 and centrifugation at 14,000 × *g* for 15 min each time. The casing pipe was replaced and 300 μL of 0.1 M NH_4HCO_3 was added before adding trypsin (Promega, V5280) with a trypsin to protein mass ratio of 1:50. The samples were incubated at 37℃ overnight. After centrifugation at 14,000 × *g* for 15 min, the supernatant was collected. 200 μL of 0.1 M NH_4HCO_3 was added, followed by centrifugation at 14,000 × *g* for 15 min. Finally, 20% TFA (Macklin, T818781) was added to acidify the sample to pH 2–3. Strata X was activated using methanol (Phenomenex, 8B-S100-AAK), and then the Strata X column was balanced with 0.1% TFA. The acidified peptides were transferred to Strata X and the hydrolysate flowed through. The salt was demineralized using 0.1% TFA and eluted once with 80% ACN. The sample was then tested on the Exploris 480 after spin-drying.

Table 2 The WB antibody information used in the present work

Antibody	Supplier, Cat no.	Dilution
CX3CR1	Novus, 76,949; Abcam, 217,291	1:1000
UCHL1	Novus, nb600-1160; Proteintech, 14730-1-AP	1:1000
FLT1	Novus, nb600-1004	1:1000
ALIX	CST, 2171 S	1:1000
TSG101	Proteintech, 28283-1-AP	1:1000
CD63	Proteintech, 67605-1-Ig	1:1000
CD9	Santa Cruz, SC-13,118	1:500
β-ACTIN	Proteintech, 81115-1-RR	1:2000
Rabbit secondary antibody	Proteintech, PR30011	1:5000
Mouse secondary antibody	Proteintech, PR30012	1:5000

Quantitative real-time-PCR (qPCR)

When the cell reached confluence, 1 mL of Trizol (Invitrogen, 15596018CN) was added to each well for extraction of total RNA. The cell lysate was collected into a 1.5 mL RNase-free EP tube. Then 0.2 mL of chloroform was added and gently shaken for 15 s. The samples were incubated at room temperature for 10 min and then centrifuged at 12,000 rpm for 10 min at 4 °C. The colorless water phase supernatant was transferred to a new 1.5 mL RNase-free EP tube. After the addition of the same amount of isopropyl alcohol, the mixture was shaken up and down. Subsequently, the samples were incubated at room temperature for 10 min and then centrifuged at 12,000 rpm for 10 min at 4 °C. After washing with 75% ethanol, the total RNA was dissolved in 20–30 μL of DEPC water. The OD value was measured using Nanodrop. The genomic DNA was removed and the RNA was reverse-transcribed into cDNA (Takara, RR047A). The primer sequence is shown in Table 1. The cDNA sample was mixed with primer and Syber Green (Takara, RR420A), and then ABI Q5 fluorescence quantitative PCR was performed for amplification.

Western blot (WB)

Equal amounts of total protein from cells or EVs were separated by 10% SDS-PAGE gels and then transferred to PVDF membranes (Millipore, ISEQ00010). The membranes were incubated with primary antibodies (listed in Table 2) overnight at 4 °C after blocking with TBST containing 5% skim milk. After washing with TBST for 10 min for 3 times, the membranes were incubated with secondary antibody for 1 h at room temperature. Bands were exposed by an enhanced Chemiluminescence detection kit (BIO-RAD, 1705062) and captured with a BIO-RAD ChemiDoc MP multi-function Chemiluminescence imager. Gray value analysis of the images was performed by ImageJ software, with β-ACTIN gray values serving as the control.

Immunofluorescence

The cells were sub-cultured on confocal dishes. When the optimal density was reached with a confluence of 25–30%, the cells were fixed with 4% paraformaldehyde (PFA) for 20 min at room temperature. After incubation with a blocking buffer (consisting of 1% BSA, 0.3% Triton X-100, and 4% normal goat serum in PBS) for 30 min at room temperature, the samples were incubated with primary antibodies against CX3CR1 (C-X3-C motif chemokine receptor 1, Novus, 76949, 1:500) and UCHL1 (Ubiquitin C-terminal hydrolase L1, Proteintech, 14730-1-AP, 1:500) overnight at 4 °C. Subsequently, the samples were incubated with fluorophore-conjugated secondary antibodies (Invitrogen, A11008, 1:1000; Invitrogen, A11035, 1:1000) for 1 h at room temperature. Nuclei were stained with a diluted DAPI (Sigma, D9542, 1:5000) solution. Immunofluorescence images were observed and captured by confocal microscopy (Olympus FV3000).

After dewaxing and hydration of paraffin-embedded tissue sections, antigen retrieval was performed using 10 mM sodium citrate (pH 6.0, Servicebio, g1201-1 L) at 120 °C for 3 min. Following 1-hour block with 1% BSA, the sections were incubated with primary antibodies against CX3CR1 (Abcam, ab167571, 1:500), UCHL1 (Proteintech, CL594-14730, 1:500), IBA1 (Abcam, ab283319, 1:500), NEUN (Abcam, ab177487, 1:500), GFAP (Proteintech, 16825-1-AP, 1:500), CC1 (Abcam, ab16794, 1:500), and CD31 (CST, 89C2, 1:500) at 4 °C overnight. Subsequently, the samples were incubated with fluorophore-conjugated secondary antibodies (Invitrogen, A32723, 1:1000; Invitrogen, A21245, 1:1000) for 2 h at room temperature after washing with PBS 3 times. Nuclei were stained with DAPI (1:5000). Immunofluorescence images were observed and captured by confocal microscopy (Leica STELLARIS 8).

EVs isolation

EVs were extracted from human plasma by an ultracentrifugation methodology as previously described [13, 14]. Briefly, the plasma was isolated from whole blood by centrifugation at 300 × *g* for 10 min at 4 °C to remove erythrocytes and at 2,000 × *g* for 15 min at 4 °C to remove platelets. 110 µL of isolated plasma was then centrifuged at 12,000 × *g* for 30 min at 4 °C to remove large cell debris. The 100 µL of supernatant was diluted with 900 µL of PBS which had been filtered through a 0.22 µm filter. The mixture was carefully balanced and ultracentrifuged at 100,000 × *g* for 70 min at 4 °C by an ultracentrifuge (Beckman Coulter Optima MAX-XP centrifuge, TLA-55 rotor). The pellet was resuspended with 1 mL of PBS and ultracentrifuged again with the same condition. The EVs were dissolved in 200 µL of PBS and stored at -80°C before detection.

EVs were extracted from the conditioned medium of cultured cells. When the cells were cultured in DMEM without FBS for 48 h, the conditioned medium was collected and centrifuged at 1,500 × *g* for 10 min at 4 °C. The supernatant was then centrifuged at 3,000 × *g* for 15 min. Subsequently, the supernatant was centrifuged at 7,800 × *g* for 30 min at 4 °C. The supernatant was further centrifuged at 200,000 × *g* at 4 °C for 2 h. The pellets were resuspended with 1 mL of PBS and centrifuged again at 200,000 × *g* at 4 °C for 2 h. The EVs were dissolved in 200 µL of PBS and stored at -80 °C before detection.

Nano flow cytometry analysis

The concentration of EVs carrying specific markers was measured according to our previous description [13, 14]. Briefly, the EVs were labeled with primary antibodies and then conjugated with fluorophores by Zenon IgG labeling kits (Invitrogen). CX3CR1 (Novus, 76949) was labeled using the Zenon Alexa Fluor 488 Rabbit IgG labeling kit (Invitrogen, Z25302). UCHL1 (Proteintech, 14730-1-AP) was labeled using the Zenon Alexa Fluor 647 Rabbit IgG labeling kit (Invitrogen, Z25308). NMDAR2A (Invitrogen, MA5-27693) was labeled using the Zenon Alexa Fluor 647 mouse IgG_{2b} labeling kit (Invitrogen, Z25208). NFL (Proteintech, 60189-1-Ig) was labeled using the Zenon Alexa Fluor 488 mouse IgG_1 labeling kit (Invitrogen, Z25002). The immunoglobulin homologous control corresponding to each antibody was also labeled under the same conditions. A negative control was included by using the same volume of PBS instead of a specific antibody during the labeling reaction. The labeled antibodies were added to 5 µL of samples (0.1 µg of equivalent antibody amount per sample) and incubated overnight at 4 °C. Afterward, the samples were fixed with 20 µL of 4% PFA at 26 °C for 20 min and then diluted to 100 µL with PBS. Finally, the samples were analyzed using the Cytoflex LX (Beckman).

Stochastic optical reconstruction microscopy (STORM)

After incubation with antibodies for 18 h, the plasma EVs were fixed with 4% PFA and then immersed in 200 µL of sample buffer (50 mM Tris-HCl, pH8.0, 10 mM NaCl, and 10% Glucose) for STORM detection. All images were obtained using the ultra-high-resolution Nikon A1 confocal total internal reflection microscope (N-STORM/A1R). The fluorophores of Alexa 561, Alexa 488, and Alexa 647 were excited by 561 nm, 488 nm, and 647 nm semiconductor lasers, respectively.

Clinical samples collection

Plasma samples from 303 subjects (78 healthy control (HC), 138 patients with MS, and 29 patients with HAM, 21 patients with AD, and 37 patients with PD) were obtained from Fujian Medical University. To further

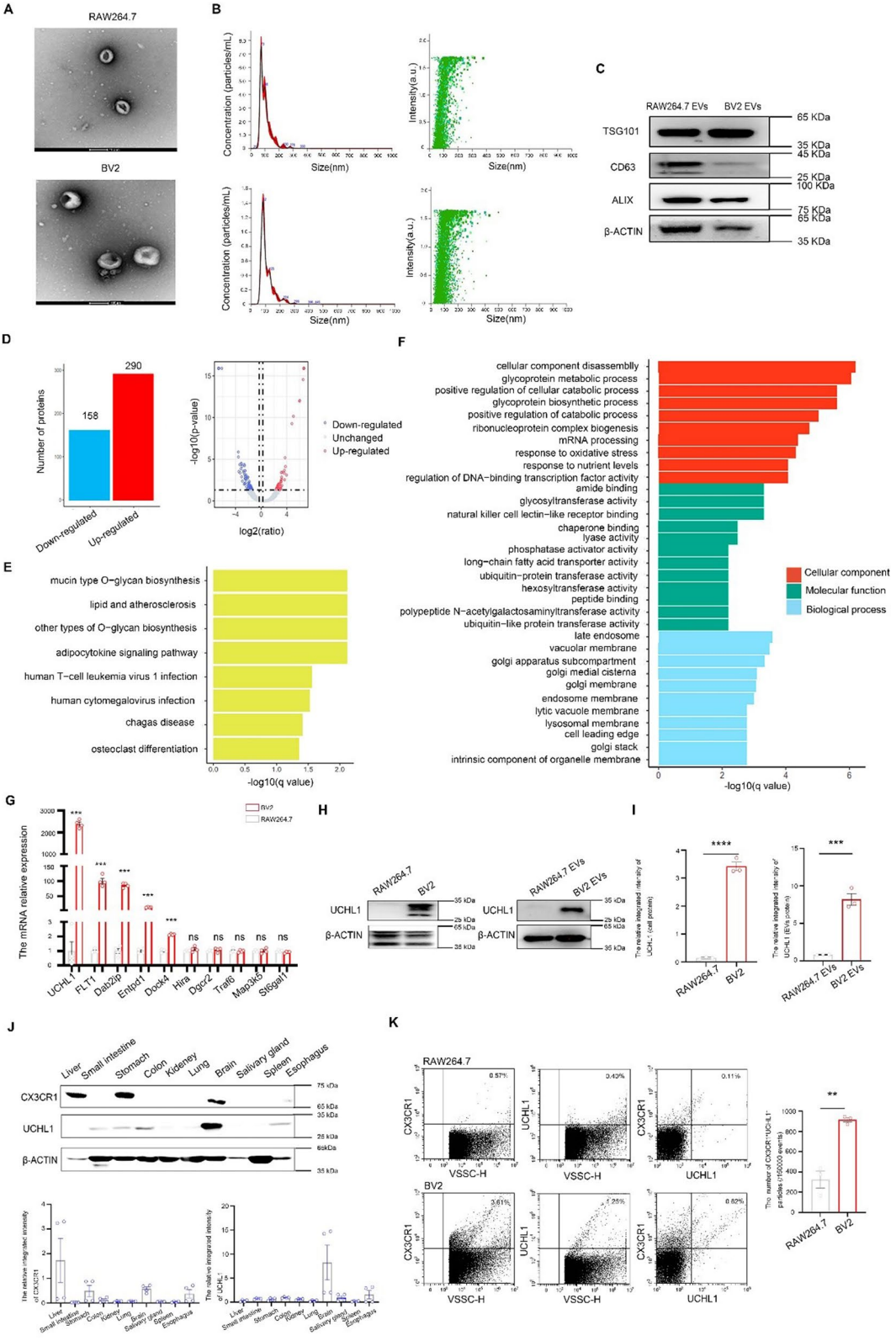

Fig. 1 (See legend on next page.)

(See figure on previous page.)

Fig. 1 UCHL1 was a highly specific protein in BV2 EVs confirmed by mass spectrum screening. (**A**) Characteristic electron microscopy images of the EVs derived from BV2 and RAW264.7. (**B**) Representative NTA images showed the population of EVs derived from BV2 and RAW264.7. (**C**) WB images showed the exosome markers (TSG101, CD63, and ALIX) expressed in the EVs of BV2 and RAW264.7. (**D**) The bar plot and Volcano plot showed the different proteins between BV2 and RAW264.7 EVs. (**E**) KEGG analysis of different proteins between BV2 and RAW264.7 EVs. (**F**) GO analysis of different proteins between BV2 and RAW264.7 EVs. (**G**) qPCR verified the top 10 of different proteins between BV2 and RAW264.7. (**H**) WB images showed the UCHL1 expression in BV2 and RAW264.7 and the EVs secreted from those cells. (**I**) Quantification of the relative integrated intensity of cell protein and EVs protein in BV2 and RAW264.7 by WB. (**J**) Typical WB images for CX3CR1 and UCHL1 and their quantification of relative integrated intensity in different mouse organs. $^{***}p < 0.001$ versus other groups. (**K**) Representative images for double labeling CX3CR1 and UCHL1, along with the quantification of double-positive particles in BV2 and RAW264.7 EVs. All values are mean ± SEM. $n = 3$–4 in each group. $^{**}p < 0.01$, $^{***}p < 0.001$, $^{****}p < 0.0001$, ns, no significance

evaluate AD and PD cohorts, additional 123 plasma samples (53 HC, 36 patients with AD, and 34 patients with PD) were obtained from The First Affiliated Hospital, Zhejiang University School of Medicine. All procedures were performed in compliance with relevant laws and institutional guidelines and approved by the appropriate institutions (Clinical Research Ethics approval no.NCT04386018 from Fujian Medical University and no.2022-043 from The First Affiliated Hospital, Zhejiang University School of Medicine), and informed consent was obtained from each patient. The privacy rights of human subjects had always been observed. MS patients were diagnosed based on the 2017 McDonald MS diagnostic criteria. Peripheral blood and the DNA of cerebral spinal fluid (CSF) was extracted to assess the HTLV-1 proviral load (PVL) in HAM patients using real-time PCR, following the HAM/TSP diagnostic criteria. All HAM patients were HTLV-1 antibody positive. AD and PD participants underwent extensive clinical evaluation, using the inclusion and exclusion criteria as well as sample collection procedures that have been previously described [22–26].

Transmission electron microscope (TEM)

The extracted EVs were suspended in PBS and dripped onto a copper grid with a pore size of 2 nm. After incubation at room temperature for 2 min, the liquid was removed from the side of the grid using filter paper, and the samples were negatively stained with a 3% phosphotungstic acid solution at room temperature for 5 min. Following the removal of excess dye and drying at room temperature, the EVs were observed and captured by the Talos 120 kV transmission electron microscope.

Nanoparticle tracking analysis (NTA)

The NanoSight NS300 instrument was utilized for nanoparticle tracking to analyze the size and concentration of particles. To conduct direct scattering measurements, 10 μL of EVs were diluted in a 1:100 ratio with 0.22 μm filtered PBS to a final volume of 1 mL. The optical microscope was used to photograph, track, and analyze the scattered light signal and Brownian motion of the collected EVs. Three repeated videos (60 s each) were captured for each fraction. All fractions were analyzed with the same threshold by the NTA 3.2 software (NanoSight, Amesbury).

The single molecule array (Simoa)

The levels of serum NFL were measured using ultra-sensitive Simoa technology (Quanterix, MA, US) on Quanterix SR-X, following the manufacturer's instructions. According to human NF-light V2 advantage kits (Quanterix, 104073), sera were diluted at a 1:4 ratio for the assay. Calibrators and quality controls were measured in duplicate. All sample measurements were performed in a single run. The operators conducting the measurements were blinded to the participants' disease status and clinical information.

Data analysis

All statistical analyses were performed by utilizing SPSS 25.0 (IBM) or Prism 9.0 (GraphPad Software). All values are presented as Mean±standard error of mean (SEM). The normality of the data distribution was assessed using the Shapiro-Wilk test. To compare the mean of total particle number (independent of any fluorescent cell type marker) or the ratio of a specific positive marker to total events for scattering tests, we employed either the Mann-Whitney U test (for two sets) or one-way nonparametric ANOVA, Kruskal-Wallis test (for three sets). ROC curves were generated to evaluate the sensitivity and specificity of the analyte in distinguishing MS from HCor HAM. Logistic regression was used to create a comprehensive model that incorporated multiple plasma biomarkers. We only used a single, relatively large cohort for this investigation, so to prevent overfitting from testing multiple parameters, we took several precautions. First, we randomly split our samples ($n=67$ for HC, 113 for MS, and 29 for HAM) into independent training and test datasets in a 4:1 ratio. On the training data, we employed two models (Linear regression [27] and Random forest [28]) and evaluated their performance using 5-fold cross-validation [29]. Finally, we evaluated the trained models on the independent test dataset using Python. A significance level of $P<0.05$ was considered statistically significant.

Results

Identification of microglial specific EVs

To identify microglial-specific EV markers, using ultracentrifugation, EVs were initially enriched from the conditioned media of BV2 microglial cell line and RAW264.7 bone marrow macrophage cell line, respectively. The EVs were characterized extensively with TEM (transmission electron microscope), NTA (nanoparticle tracking analysis), and WB (Western blot) techniques. TEM imaging revealed that the isolated components exhibited cup-shaped or vesicular morphology with diameters ranging from approximately 30 nm to 150 nm (Fig. 1A). NTA studies indicated that the primary peak particle size of EVs derived from BV2 cells was 108.3 nm, while the size of EVs derived from RAW264.7 cells was 101.8 nm (Fig. 1B). Furthermore, WB results confirmed the presence of typical EV markers such as CD63, ALIX, and TSG101 (Fig. 1C). These results collectively demonstrated the characteristic of the isolated EVs from both cell lines.

With the EVs characterized above, the protein profiles were analyzed using unbiased mass spectrometry. As depicted in the bar plot and volcano plot (Fig. 1D), we identified 290 uniquely upregulated and 158 downregulated proteins in BV2-derived EVs compared to RAW264.7-derived EVs. KEGG analysis demonstrated that these differential genes were primarily enriched in glucose and lipid metabolism pathways (Fig. 1E). Furthermore, GO analysis revealed that the corresponding differential genes were intimately associated with cell composition, glucose metabolism, oxidative stress, and Golgi apparatus organization (Fig. 1F).

When comparing the mass-spectrometry results with the Human Protein Atlas database (https://www.proteinatlas.org/), we identified the top 10 microglial-specific proteins that were highly expressed in BV2-derived EVs but not in RAW264.7-derived EVs (Table 3). Among these differential proteins, UCHL1 emerged as a promising candidate for distinguishing microglial EVs from those of macrophages. This is supported by elevated gene expression quantified by qPCR (Fig. 1G) and a pronounced increase in UCHL1 protein expression in BV2 cells compared to RAW264.7 cells and their associated EVs (Fig. 1H, I) as shown by WB results. Together, these results suggest that UCHL1 could potentially serve as a specific protein to distinguish microglia from macrophages.

On the other hand, it is known that UCHL1 is not expressed exclusively in microglia. Indeed, the WB results showed that the expression of UCHL1, while relatively higher in the brain compared to other organ tissues in adult mice, was not unique to the brain (Fig. 1J). To isolate microglial EVs more specifically, we utilized a nano flow cytometry platform that identifies a microglial population using double biomarkers. Specifically, in the following series of investigations, in addition to UCHL1, we added CX3CR1, a protein co-expressed uniformly and specifically in both microglia and macrophages for the definition of microglia EVs. As shown in Fig. 1K, CX3CR1 and UCHL1 double-positive particles in EVs secreted by BV2 were significantly more abundant than those in EVs secreted by RAW264.7.

To substantiate the specificity of CX3CR1 and UCHL1 beyond cell line cultures, we conducted qPCR, WB, and immunofluorescence analyses on primary cultured microglia and macrophages. For the CX3CR1, although gene expression was significantly higher in primary microglia than in primary cultured macrophages at the qPCR level (Fig. 2A), WB analysis, immunofluorescence, and flow cytometry showed comparable levels of CX3CR1 expression in both cell types (Fig. 2B, C, D). On the other hand, consistent with our previous results, the mRNA levels of *Uchl1* in primary cultured microglia were significantly higher than those in primary cultured macrophages (Fig. 2A). Furthermore, both WB and immunofluorescence staining also confirmed that the protein expressions of UCHL1 in primary microglia were notably higher than those in primary macrophages

Table 3 The differential genes between BV2 and RAW264.2 screened by mass spectrum

Confidence	Accession	Description	Coverage [%]	MW [kDa]	BV2/RAW264.7	*p* value
High	P35969	FLT1	4	149.8	100	1.23929E-16
High	Q9R0P9	UCHL1	14	24.8	100	1.23929E-16
High	P59764	DOCK4	1	226.4	100	1.23929E-16
High	O35099	MAP3K5	3	154.4	100	1.23929E-16
High	Q61666	HIRA	4	111.7	100	1.23929E-16
High	P98154	DGCR2	2	60.7	100	1.23929E-16
High	P70196	TRAF6	2	60	100	1.23929E-16
High	Q64685	ST6GAL	4	46.6	100	1.23929E-16
High	Q3UHC7	DAB2IP	3	131.6	100	1.23929E-16
High	Q9R0A0	PEX14	3	41.2	100	1.23929E-16

Note Coverage (%) represents how much percentage that the peptides fraction identified by mass spectrometry took up in the whole protein. MW=Molecular weight. Because the signals for certain proteins can be detected in BV2 EVs via mass spectrometry but not in RAW 264.7 EVs, the system defaults the fold change (BV2/RAW264.7) to 100

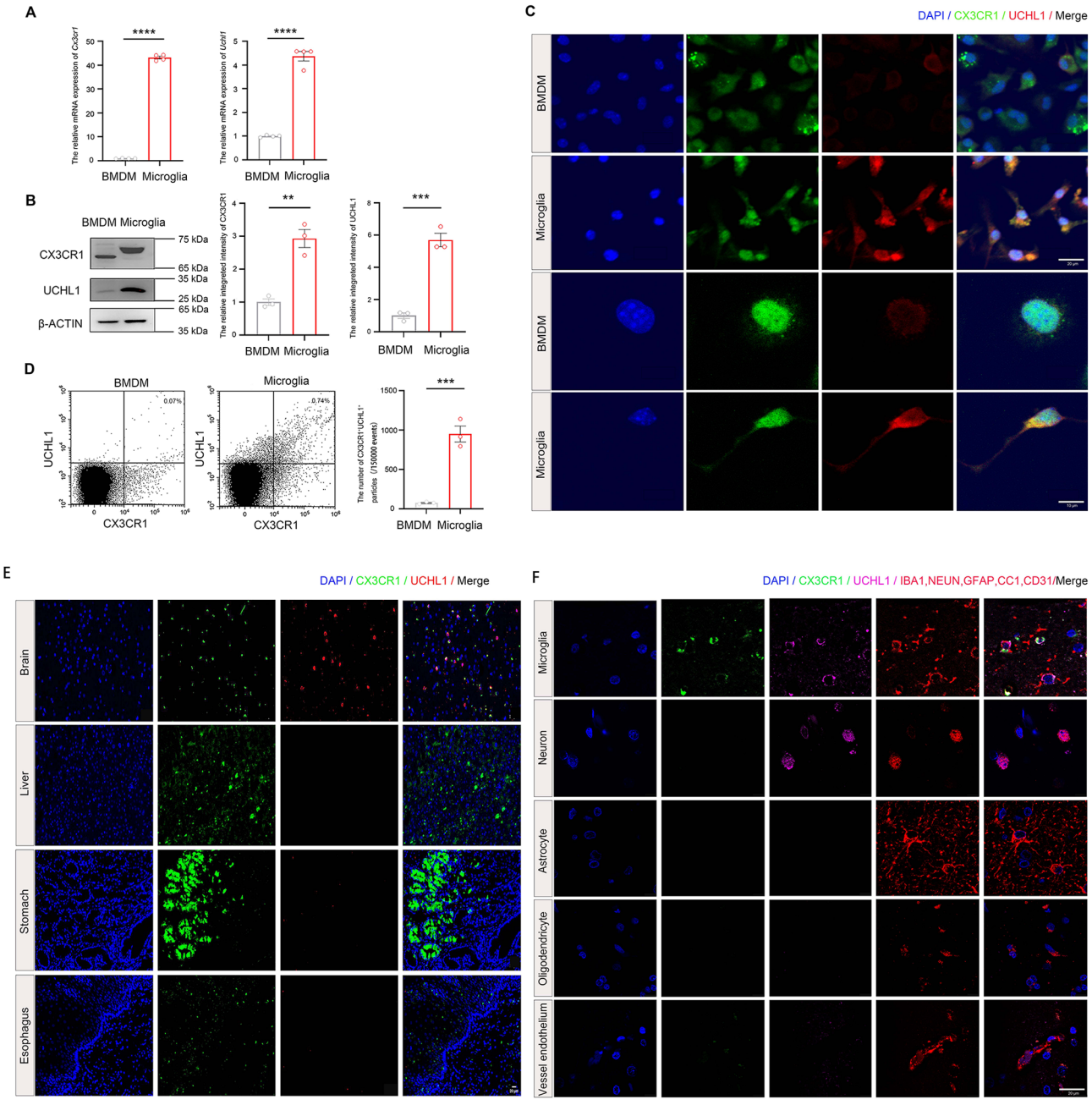

Fig. 2 Specific co-expression of CX3CR1 and UCHL1 in microglia. (**A**) Quantification of the relative mRNA expressions of *Cx3cr1* and *Uchl1* in primary cultured Bone marrow-derived macrophage (BMDM) and microglia by qPCR. (**B**) Representative images of WB showed the expression of CX3CR1 and UCHL1 in primary cultured BMDM and microglia. (**C**) Representative immunostaining images for CX3CR1 and UCHL1 in primary cultured BMDM and microglia. (**D**) Images for double labeling CX3CR1 and UCHL1 in the EVs from BMDM and microglia and quantification of the double positive particles by Cytoflex LX. (**E**) Representative immunostaining images for CX3CR1 and UCHL1 in human brain, liver, stomach, and esophagus sections. (**F**) Representative immunostaining images for CX3CR1 and UCHL1 colocalization in different cell types (IBA1 for microglia, NEUN for neuron, GFAP for astrocyte, CC1 for oligodendrocyte, CD31 for brain microvascular endothelial cells) in human brain sections. All values are mean ± SEM. $n = 3–4$ in each group. $^{**}p < 0.01$, $^{***}p < 0.001$, $^{****}p < 0.0001$

(Fig. 2B, C). Finally, nano flow cytometry results showed a remarkable enrichment of UCHL1$^+$/CX3CR1$^+$ particles in primary microglial EVs compared to those in primary macrophage EVs (Fig. 2D).

To validate the specificity of co-labeling of CX3CR1 and UCHL1 as unique microglial markers, two additional investigations were conducted. First, at organ level, as expected, CX3CR1 and UCHL1 are not only expressed in brain tissue but also in the liver, stomach, and esophagus

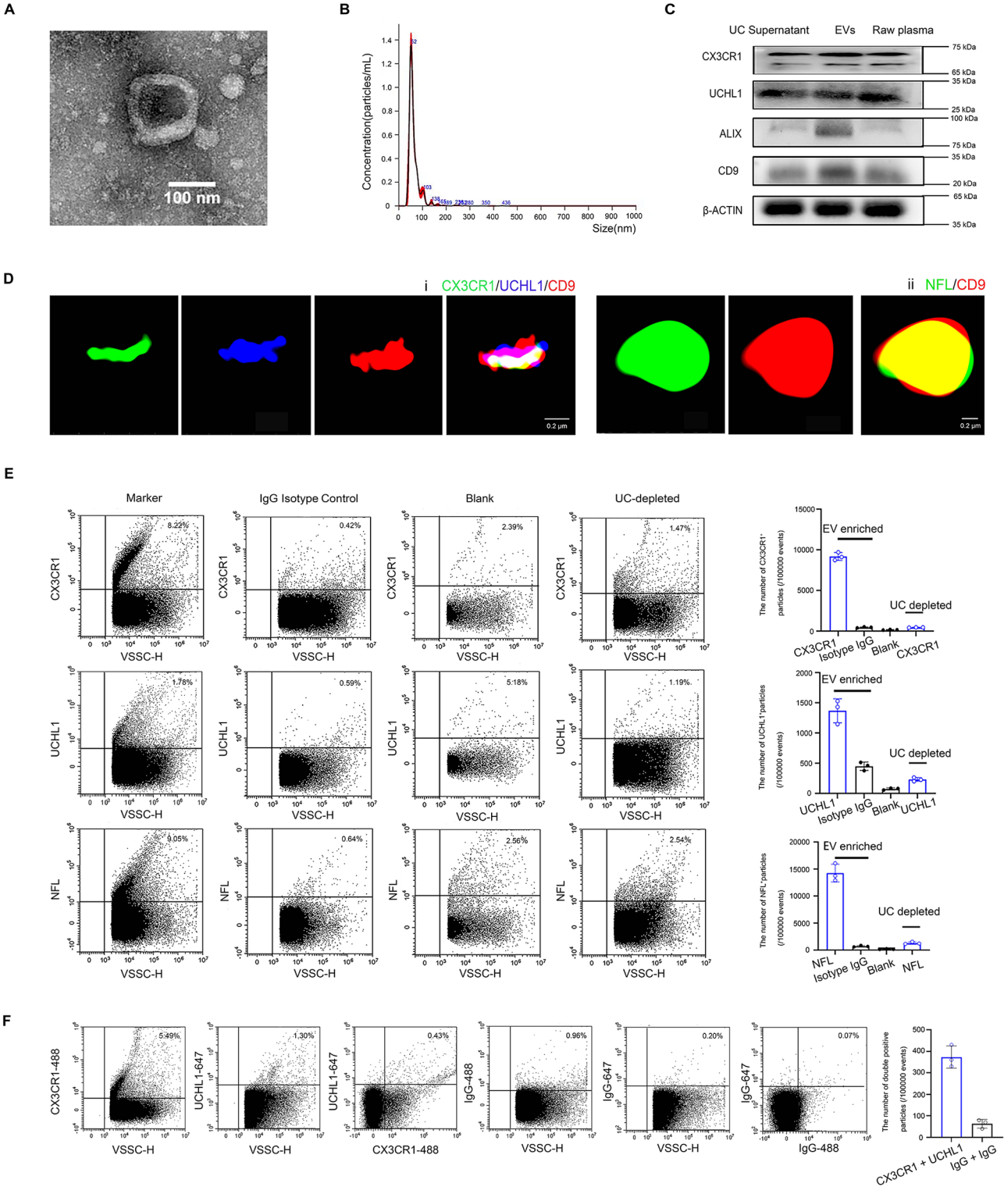

Fig. 3 (See legend on next page.)

of mice (Fig. 1J), however, the highest co-localization of both proteins was in the brain (Fig. 2E). At cellular level to evaluate the cell types co-localized with CX3CR1 and UCHL1 in the brain, we performed immunofluorescent staining for CX3CR1, UCHL1, and cell markers (IBA1, NEUN, GFAP, CC1, and CD31) using human brain tissue sections. The results demonstrated that co-localization of CX3CR1 and UCHL1 was only present in IBA1-positive

(See figure on previous page.)

Fig. 3 Characterization of microglia-derived EVs in human plasma. (**A**) A representative. TEM image of EVs isolated from human plasma showed double-layered membrane-bound vesicles. (**B**) NTA showed a population of EVs with a peak around 70 nm. (**C**) Representative images of WB showed the expression of microglia-specific markers (CX3CR1 and UCHL1) and EV markers (ALIX and CD9) in the isolated EVs from plasma, raw human plasma and the supernatant of plasma ultracentrifugation. (**D**) Typical STORM images showed CX3CR1 and UCHL1 colocalized on the CD9 marked EV membranes. Moreover, NFL was localized on the CD9-marked EV membranes. Notably, the size of EV signals in STORM exceeds 200 nm, which may be attributed to PFA fixation and the algorithm-based approach, both of which introduce certain biases when characterizing the size of EVs. (**E**) Representative histograms showed the populations of EVs positive for each marker (CX3CR1, UCHL1, and NFL), fluorophore-conjugated IgG isotype control, a blank (fluorophore only, no antibody) control experiment, and UC-depleted (plasma with depletion of EVs by ultracentrifugation). Quantification data of positive EVs detected by the flow cytometry-based assay demonstrating the specificity of EV assays. (**F**) Representative images for double labeling of microglial EV markers (CX3CR1 and UCHL1) and isotype IgG in a pooled human plasma sample (combined plasma from 40 individuals). All values are mean ± SEM. $n = 3$ in each group

microglial cells (Fig. 2F). These findings cooperatively underscore the development of a novel biomarker for distinguishing microglia from macrophages.

Characterization of microglial EVs in human plasma

To probe the possibility of microglia-derived EVs as a biomarker for neurological disorders, we optimized a strategy to capture microglia-derived EVs from human plasma, with the method developed previously in our lab [13]. EVs extracted from human plasma were observed by TEM after ultracentrifugation to analyze their morphology and size. The double-layer membrane structure, with a diameter of about 30–150 nm, was observed in cup-shaped or vesicular-shaped EVs (Fig. 3A). NTA results showed that the enrichment peak was about 70 nm (Fig. 3B). Furthermore, WB results showed that the EVs from plasma concurrently contained EV markers (ALIX and CD9) and microglial markers (CX3CR1 and UCHL1) (Fig. 3C).

To further validate the identification of microglial-derived EVs from human plasma, an ultra-high resolution imaging technique (STORM) was employed. The results showed that microglial markers CX3CR1 and UCHL1 were co-localized with exosome marker CD9 on the membrane of EVs (Fig. 3D i). Additionally, co-localization of NFL, a marker commonly used in MS progression analysis, was also observed together with CD9 on EVs (Fig. 3D ii). Another synaptic-associated protein, NMDAR2A, a neuronal EV marker, has been previously verified by our laboratory to co-localize with CD9 [13].

To develop a practical method to robustly measure CX3CR1 and UCHL1 double-positive microglial EVs in plasma, we further optimized the nanoscale flow cytometry assay used routinely in our lab. The results showed that $CX3CR1^+$, $UCHL1^+$, and NFL^+ EVs were clearly detectable in plasma, with only a small amount of positive signal detected in the isotype IgG control group, blank group, and EVs-depleted plasma (Fig. 3E). Further study with nano flow cytometry indicated that the CX3CR1 and UCHL1 double-positive particles were precisely captured in human plasma EVs (Fig. 3F). For stability and reproducibility testing, the antibodies of CX3CR1, UCHL1, and NFL were diluted with four different dilution ratios (1:25, 1:50, 1:100 or 1:200) and the same test was performed for 5 consecutive days. The results showed that these antibodies had a stable labeling percentage of EVs with different dilution ratios and different testing time points (Supplementary Fig. S2). The standard sample (fluorescent beads of known size) was run periodically to calibrate the differences between batches. All the above results proved the labeling assay had reasonable stability and reproducibility.

Microglial EVs in the diagnostics of MS

To explore potential clinical applications of the newly developed microglial EVs markers, we preliminarily explored the levels of these markers in several representative neurodegenerative diseases, including MS, AD, and PD, all of which involve some degree of neuroinflammation. This analysis included 25 MS patients, 21 AD patients, 37 PD patients, and 11 HC from Fujian Medical University. Clinical characteristics are shown in Table 4. Notably, the number of $CX3CR1^+/UCHL1^+$ EVs was significantly increased in the plasma of the MS group, while it did not change significantly in AD or PD patients compared to the HC group (Supplementary Fig. S3). Next, we focused on MS, using HAM as a relevant disease control group due to its clinical similarity to MS. Samples were selected based on clinical diagnostic criteria and included MS (multiple sclerosis, $n = 113$), HAM (HTLV-1-associated myelopathy, $n = 29$), and HC (healthy control, $n = 67$). The characteristics of the clinical cohorts are summarized in Table 5.

Using $CX3CR1^+/UCHL1^+$ EVs as the microglial EV markers, our results indicated a significant increase in $CX3CR1^+/UCHL1^+$ EVs in the MS group when compared to the HC group. Notably, the HAM group exhibited even higher numbers of microglial EVs compared to the MS group (Fig. 4A). Recognizing the potential neurodegenerative aspects in MS due to axonal degeneration alongside demyelinating lesions, we also included the EVs containing the synaptic-associated protein NMDAR2A, which decreases in AD significantly [13], and the EVs containing axon protein NFL, a marker commonly used to reflect neurodegeneration [30, 31], to assess the extent of neurodegenerative response. Remarkably, the

Table 4 Summary of the demographics and clinical data of MS, AD, PD, and HC participants from Fujian Medical University

	HC	MS	AD	PD
Case no	11	25	21	37
$CX3CR1^+$/$UCHL1^+$ (%)	0.26 ± 0.11	0.58 ± 0.45	0.24 ± 0.10	0.31 ± 0.12
Age	mean = 32.48 range: 23–62	mean = 39.5 range:20–60	mean = 62.43 range: 49–77	mean = 67.19 range: 47–78
Sex (male: female)	6:5	10:15	8:13	25:12

Note $CX3CR1^+$/$UCHL1^+$ (%) are presented by mean ± SEM

Table 5 Summary of the demographics and clinical data of MS and HAM participants

	HC	MS	HAM
Case no	67	113	29
$CX3CR1^+UCHL1^+$ (%)	0.24 ± 0.11	0.34 ± 0.39	0.65 ± 0.37
NMDAR2A (%)	1.22 ± 0.57	2.21 ± 1.01	3.69 ± 1.54
NFL (%)	1.43 ± 0.76	2.15 ± 1.25	3.69 ± 1.94
Age	mean = 25.86 range: 22–40	mean = 35.41 range: 9–71	mean = 50.07 range: 33–61
Sex (male: female)	10:57	32:81	5:24
Disease duration (year)	---	mean = 7.1 range: 0.1–23	mean = 10.04 range: 0–20
EDSS	---	3.1 ± 1.9	4.19 ± 1.33
Subtype (RRMS: PPMS: SPMS)	---	95:10:8	---
NFL (Simoa, pg/mL, $n = 70$)	---	25.13 ± 38.85	---
CSF HTLV-1 antibody	---	---	All (+)
Plasma HTLV-1 antibody	---	---	All (+)
PBMC virus titers	---	---	10.87 ± 6.89

Note $CX3CR1^+$/$UCHL1^+$ (%), NMDAR2A (%), NFL (%), EDSS, NFL (Simoa, pg/mL, $n = 70$), and PBMC virus titers in the table are presented as mean ± SEM. EDSS = Expanded Disability Status Scale, RRMS = Relapsing Remitting Multiple Sclerosis, PPMS = Primary Progressive Multiple Sclerosis, SPMS = Secondary Progressive Multiple Sclerosis, CSF = Cerebrospinal Fluid, PBMC = Peripheral Blood Mononuclear Cell

proportion of NMDAR2A- and NFL-positive EVs in the peripheral blood of MS patients was significantly higher compared to the HC group. Furthermore, the HAM group exhibited even higher levels of microglial EVs in comparison to the MS group, especially in the portion of the particles < 150 nm (Fig. 4B, C), i.e., those within the size of typical exosomes.

The ROC analysis was carried out to evaluate the diagnostic performance of $CX3CR1^+$/$UCHL1^+$ EVs in differentiating patients with MS from HC or patients with HAM. Comparing patients with MS and HC, the AUC (Area Under the Curve) analysis value was 0.72 (95% CI = 0.63–0.81) for $CX3CR1^+$/$UCHL1^+$ EVs, 0.86 (95% CI = 0.80–0.92) for $NMDAR2A^+$ EVs, and 0.70 (95% CI = 0.61–0.78) for NFL^+ EVs, respectively (Table 6). Although the performance of $CX3CR1^+$/$UCHL1^+$, $NMDAR2A^+$ or NFL^+ EVs alone was modest in distinguishing MS from HC, the integrative analysis combining all these biomarkers, a method commonly used in flow cytometry, further increased the diagnostic power in distinguishing MS from HC with an AUC of 0.89 (Fig. 4D; Tables 6 and 95% CI = 0.83–0.94). Similarly, the integrative model also amplified the diagnostics in differentiating MS from HAM with an AUC of 0.92 (Fig. 4E; Tables 6 and 95% CI = 0.84–0.98). To avoid overfitting from using a single cohort with multiple parameters, the cohort was randomly split into the training and test datasets, respectively, at a ratio of 4:1, followed by cross-validation analysis [29] (with two models, linear regression [27] and random forest [28]). The results largely replicated those from the logistic regression analysis (Supplementary Fig. S4). It is also important to note that the diagnostic values were not affected when age differences among different groups were factored in (Supplementary Fig. S5).

Having established the role of $CX3CR1^+$/$UCHL1^+$ EVs in diagnosing MS and differentiating it from HAM, we focused on the earlier observation that microglial EVs did not change significantly in AD or PD compared to HC (Supplementary Fig. S3), despite both diseases being associated with clear neuroinflammation. Given the limited sample size of the cohort from Fujian Medical University, we collected another set of samples, including 36 AD patients, 34 PD patients, and 53 HC, from the First Affiliated Hospital of Zhejiang University for validation. The clinical characteristics are shown in Table 7. The results of this cohort indicated that, consistent with the preliminary study, the number of $CX3CR1^+$/$UCHL1^+$ EVs did not differ in PD patients but decreased significantly in AD patients compared to HC (Supplementary Fig. S6).

Taken together, these data demonstrate that combining $CX3CR1^+$/$UCHL1^+$, $NMDAR2A^+$, and NFL^+ EVs from plasma displays a potential capability to distinguish MS from HC and HAM, but the peripheral response of microglial EVs to various neurological disorders are quite different.

Microglial EVs over the duration of MS

MS patients progress clinically, but unpredictably, during the disease duration. We analyzed the EV markers with MS disease duration for at least 10 years. Intriguingly, there were no clear trends in these EV markers (data not shown) over the duration of 10 years. Given that MS has a higher probability of clinical progression after the initial five years [32], next, we selected the first five years as a cutoff point. Remarkably, different trends in EV biomarkers were observed among MS patients between the 0–5 year and 5–10 year intervals. Specifically, the microglial $CX3CR1^+$/$UCHL1^+$ EVs showed an increasing trend in the first five years after the onset of MS symptoms but became stable in the following five years. In the patients

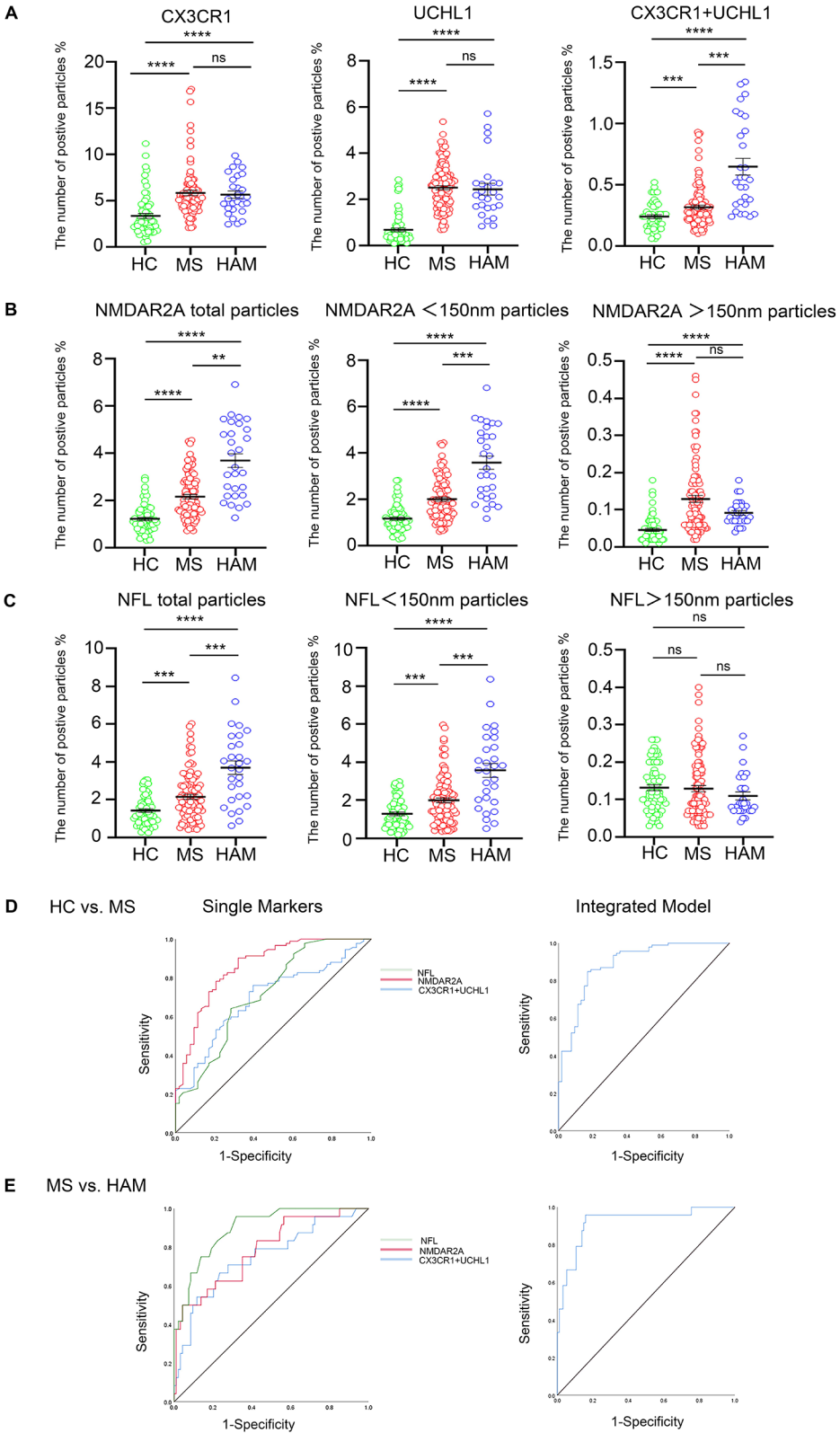

Fig. 4 (See legend on next page.)

(See figure on previous page.)

Fig. 4 Performance of CX3CR1$^+$/UCHL1$^+$, NMDAR2A$^+$, and NFL$^+$ EVs in MS cohort. The percentage of biomarker-positive particles in the total of 150,000 particles counted by nano flow cytometry is shown in the graphs. (**A**) The percentage of CX3CR1$^+$/UCHL1$^+$ EVs was significantly higher in MS than in HC, and remarkably lower in MS than in HAM. (**B**) The percentage of NMDAR2A$^+$ EVs was significantly higher in MS than in HC, and markedly lower in MS than in HAM. (**C**) The percentage of NFL$^+$ EVs was significantly higher in MS than in HC, and markedly lower in MS than in HAM. (**D**) ROC curves showed the separation of MS from HC using EVs carrying CX3CR1 + UCHL1, NMDAR2A and NFL. An integrative model including all EV markers distinguishes MS from HC. (**E**) ROC curves showed the separation of MS from HAM using EVs carrying CX3CR1 + UCHL1, NMDAR2A and NFL. An integrative model including all EV markers distinguishes MS from HAM. All values are mean ± SEM. $n = 67$ for HC, 113 for MS, and 29 for HAM. $^{**}p < 0.01$, $^{***}p < 0.001$, $^{****}p < 0.0001$, ns, no significance

with HAM, however, the CX3CR1$^+$/UCHL1$^+$ EVs did not alter significantly during the whole duration of 20 years (Fig. 5A). On the other hand, for the neurodegenerative markers, NMDAR2A$^+$ and NFL$^+$ EVs showed a relatively stable trend within the first five years after the onset of MS, while gradually increasing in the next five years. Conversely, for the patients with HAM, NMDAR2A$^+$ and NFL$^+$ EVs showed a consistently decreasing trend over the duration of 20 years (Fig. 5B, C).

Discussion

The current study represents significant progress on multiple fronts. Primarily, the investigation successfully pinpointed a distinctive combination of UCHL1 and CX3CR1 markers, allowing for the precise identification of EVs originating from CNS microglia in human blood. Furthermore, the study illustrated the potential diagnostic utility of combining microglia-derived EVs with neuron-derived EVs for both diagnosing and differentiating MS and related disorders. Lastly, the integration of microglial EVs with neuronal EVs may be useful for monitoring the disease duration of MS.

Distinguishing between microglia and macrophages in CNS research has posed a significant hurdle. Traditionally, microglia have been considered the resident CNS macrophages due to their shared origin and developmental process [33]. However, as mentioned earlier, recent studies challenge this notion, revealing that microglia and macrophages may derive from distinct sources expressing different genes or proteins [19, 34]. For example, transcriptional analysis shows that microglia and macrophages have different characteristics, despite sharing some common antigens, including CX3CR1, CD11b, and CD45 [35, 36]. Some studies have identified several proteins, including TMEM119, P2RY12, SALL1, and HEXB, as specific to microglia [37–40]. Nevertheless, our results indicated that most, if not all, of those reported "microglial specific genes/proteins" were not only expressed in microglia-derived but also macrophage-derived EVs (Supplementary Fig. S7). To clearly distinguish between EVs derived from microglia and those from macrophages, we initiated an unbiased screening process using mass spectrometry to analyze the distinctive protein profiles in EVs released from BV2 microglia and RAW264.7 macrophage cell lines. Our findings uncovered specific proteins were expressed exclusively in microglial EVs when compared to those from macrophages (Fig. 1). After further refinement, UCHL1 emerged as the primary candidate.

Proximity proteomics analysis identified that UCHL1 was an essential regulator of NLRP3-mediated IL-1β production in human microglia [41]. However, UCHL1 is not exclusively expressed in microglia. Indeed, UCHL1 is a multifunctional protein highly expressed in the brain and spinal cord, especially in neurons, playing an important role in regulating the level of cellular free ubiquitin, redox state, and the degradation of select proteins [42]. To mitigate potential interference from EVs transporting UCHL1 released by other cell types, we employed a dual labeling approach, i.e., co-labeling UCHL1 with CX3CR1, a shared robust marker for microglia and macrophages. This strategy enhanced the precision of identifying microglia-specific EVs in cell lines, primary microglia, and ultimately in human brain tissue (Figs. 1 and 2).

To determine whether microglia-derived EVs in peripheral blood could serve as potential diagnostic markers for various neurodegenerative diseases involving neuroinflammation [43, 44], we assessed their performance in patients with MS, HAM, AD, and PD. Remarkably, while alterations in microglial EVs were rather consistent in MS patients, the peripheral identification of microglia-derived EVs in other neurological diseases exhibited significant variations. In the cohort from Fujian Medical University, compared to HC, HAM patients demonstrated a substantial increase in microglial markers (see below for further discussion), whereas neither AD nor PD exhibited significant changes (Supplementary Fig. S3). Given these unexpected results on AD and PD, considering the well-documented activation and clustering of microglia around aggregated proteins like β-Amyloid (Aβ) plaques in AD [45, 46], another cohort study from the First Affiliated Hospital of Zhejiang University was performed for verification. The results of this cohort showed a significant decrease in microglial EVs in AD (Supplementary Fig. S6), with no significant differences between PD and other groups. What distinguishes CNS neuroinflammation associated with MS or HAM from the neuroinflammation unequivocally linked to AD [47] or PD [48]? The question is rather difficult to answer because the elevated peripheral microglial EVs in MS and HAM might be due to CNS microglial activation, altered synthesis or trafficking of EVs, and a compromised BBB.

Table 6 AUC value in ROC analysis (logistic regression analysis)

Marker	Comparison					
	MS vs. **HC**		**MS** vs. **HAM**		**HC** vs. **HAM**	
	AUC	**95% CI**	**AUC**	**95% CI**	**AUC**	**95% CI**
CX3CR1 + UCHL1	0.72	0.63–0.81	0.88	0.80–0.95	0.79	0.70–0.88
NMDAR2A	0.86	0.80–0.92	0.78	0.69–0.88	0.96	0.92–0.99
NFL	0.70	0.61–0.78	0.74	0.63–0.85	0.86	0.77–0.95
Combine	**0.89**	**0.83–0.94**	**0.92**	**0.84–0.98**	**0.96**	**0.92–1.00**

Note AUC = Area under the curve, CI = Confidence interval

Table 7 Summary of the demographics and clinical data of AD, PD, and HC participants from the First Affiliated Hospital of Zhejiang University

	HC	AD	PD
Case no	53	36	34
$CX3CR1^+/UCHL1^+$ (%)	0.52 ± 0.49	0.35 ± 0.33	0.37 ± 0.27
Age	mean = 68.78 range: 50–91	mean = 81.44 range: 61–96	mean = 72.69 range:36–89
Sex (male: female)	31:22	28:8	14:20

Note $CX3CR1^+/UCHL1^+$ (%) are presented by mean ± SEM

MS, a chronic autoimmune disease, is characterized by demyelination and a significant increase in microglial populations within active lesions [49]. Microglia clear myelin debris [50] and release EVs containing inflammasome components, recruiting inflammatory cells [51]. In contrast, HAM is driven primarily by microglial activation linked to HTLV-1 proviral DNA levels [52]. HTLV-1-infected CD4 T cells, secreting IFN-γ, trigger microglial activation via CD8 T cell recognition [53].

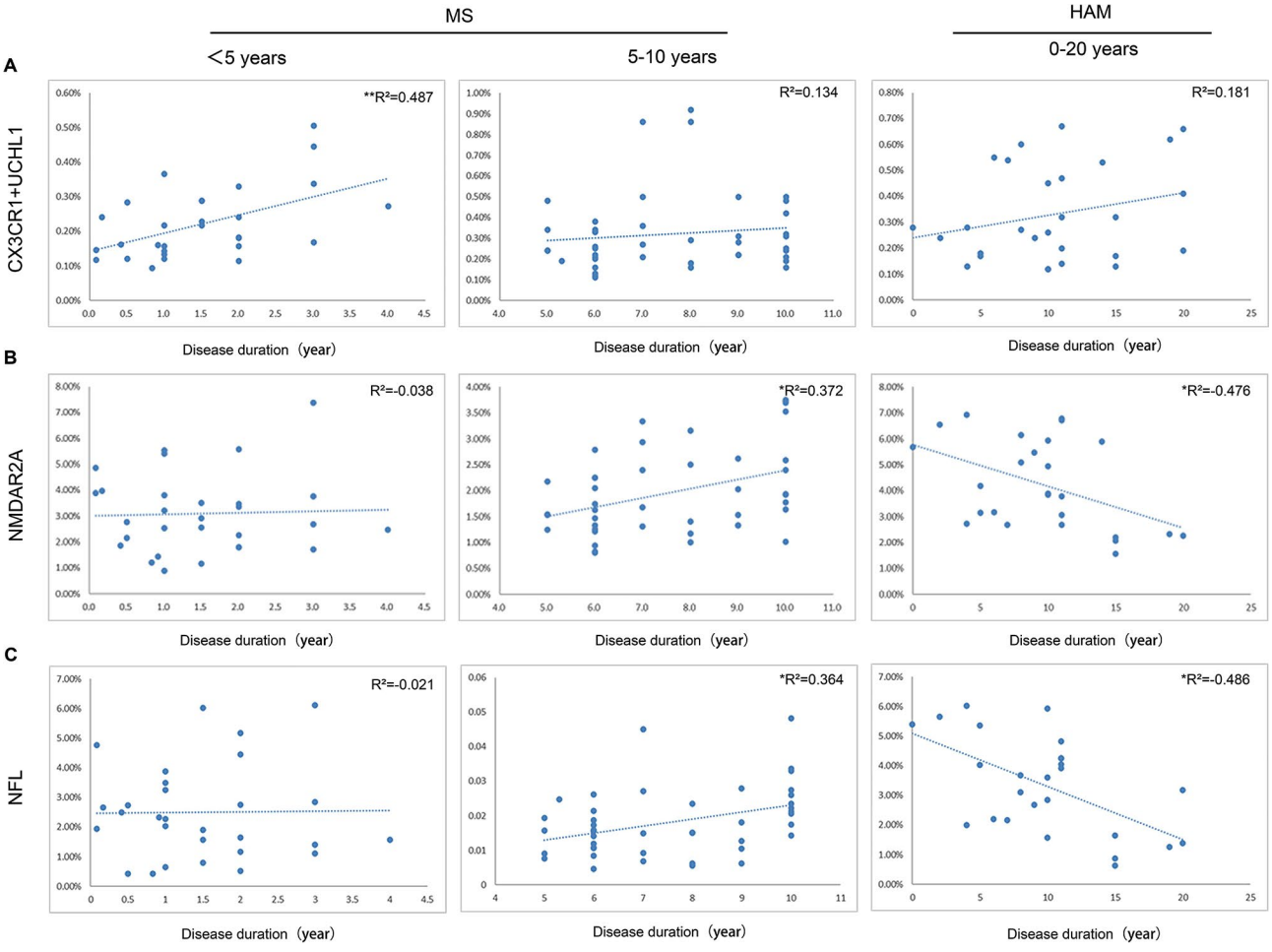

Fig. 5 Analysis of the disease duration of microglia- and synapse-derived EVs in MS and HAM. (**A**) The relationship between the number of $CX3CR1^+/UCHL1^+$ particles and disease duration in MS and HAM. (**B**) The relationship between the number of $NMDAR2A^+$ particles and disease duration in MS and HAM. (**C**) The relationship between the number of NFL^+ particles and disease duration in MS and HAM. $n = 54$ for MS and 28 for HAM. $^*P < 0.05$ and $^{**}P < 0.01$

Given the distinct pathophysiology of MS and HAM, the level of microglial activation and subsequent secretion of $CX3CR1^+/UCHL1^+$ EVs into the peripheral blood likely differ (Fig. 4A).

The integrity of BBB is another critical factor to consider. The BBB dysfunction in HAM is more severe than that in MS, which might be due to the susceptibility of cerebral endothelial cells to retroviral infection, thereby disrupting the expression of tight junctions in brain endothelial cells [54], and resulting in higher levels of microglial EVs in peripheral blood of HAM compared to MS. However, the hypothesis can be disputed readily as AD and PD are both linked to BBB dysfunction, yet without displaying an elevation in microglial EVs in blood EVs. Regardless of the underlying pathogenesis explaining the observed differences in microglial EVs in the peripheral blood of various neurological diseases, nevertheless, it is evident that these newly identified markers offer significantly improved differential power (Fig. 4, S3 and S6) in distinguishing MS from HAM, AD, PD, and HC.

The differentiation of MS from HAM using newly identified microglial EV markers is crucial, as HAM patients often manifest similar myelopathy symptoms and imaging changes to those observed in progressive forms of MS [55]. Remarkably, a significant number of HAM patients initially receive a diagnosis of primary progressive MS (PPMS). Currently, the detection of peripheral PVL in CSF serves as the primary method to diagnose HAM [56], with no other sufficiently reliable biomarker available to distinguish HAM from typical PPMS. In essence, the newly identified microglial EV markers not only contribute to confirming an MS diagnosis but also play a potential role in facilitating the differential diagnosis of MS from HAM.

As mentioned earlier, neurodegeneration develops invariably during the duration of MS progression [57]. Recent studies suggest that blood-free NFL performs reasonably well in assessing MS disease progression, however, different or better progression markers are necessary [58]. In this study, we extended our analysis to include the synaptic protein $NMDAR2A^+$ EVs and the axon-related protein NFL^+ EVs in plasma, aiming to achieve two goals. First, these markers enhanced the ability to distinguish between MS and HC or individuals with HAM (Fig. 4). The other major advantage of including neuronal markers is the increased ability to measure MS progression more objectively. Explicitly, when assessing microglia-derived EVs alone, the markers showed an upward trend within the first five years after the onset of MS symptoms, becoming stable in the next five years (Fig. 5). This pattern differs from the performance of the markers in HAM patients, where a more extended increase was observed over the entire disease duration. The mechanisms underlying this difference remain to be investigated, however, it might be attributed to abnormal phosphorylation of neurofilaments and the stripping of synaptic proteins in cortical callosal projecting neurons. Support for this hypothesis can also be found in our study, where EVs carrying NMDAR2A or NFL displayed a relatively stable pattern within the first five years of MS and then exhibited a gradual increase in the subsequent five years (Fig. 5), signifying that the disease is progressing toward neurodegeneration later in the duration of MS when the release of microglial EVs from the CNS was stabilized [59]. On the other hand, it is obvious that the MS type of neurodegeneration is different from what is observed in the plasma of HAM patients, likely due to more extensive neurodegeneration, similar to what we have observed in AD patients [60]. It is also crucial to note that the EV forms of NFL are well-correlated with the free forms of NFL in MS patients during disease progression, although the direction of changes is opposite (Supplementary Fig. S8). These results indicate that the transformation of NFL^+ EVs and free-form NFL in plasma is related to the underlying mechanisms of disease progression, clearly warranting further investigation.

The present study has several limitations: (1) The limited number of cases for AD, PD, and HAM necessitates the inclusion of more patients, particularly those recruited from multiple medical centers, to validate the preliminary results reported in this study pertaining to clinical cohorts. (2) The average ages of the HC, MS, and HAM cohorts are statistically different. We have confirmed that the percentage of $CX3CR1^+/UCHL1^+$ EVs had no relationship with age in MS, HAM, or HC (Supplementary Fig. S5), and secondary analysis also addressed this issue again through covariable analysis (p ($CX3CR1^+/UCHL1^+$)=0.079, p ($NMDAR2A^+$)=0.461, p (NFL^+)=0.697). However, efforts should be made to minimize age differences in future studies. (3) There are several subtypes of MS, including RRMS and SPMS, but there are no clear clinical, imaging, immunologic, or pathologic criteria to confidently delineate patient progression from RRMS to SPMS [61, 62]. This issue is further complicated by the fact that most of the MS patients in our cohort had RRMS, limiting our ability to correlate microglial markers with different MS subtypes. Future studies should investigate the association between microglial EVs and MS subtypes in better-characterized cohorts, including those with longitudinal follow-up, to identify and assess progression markers and explore how these markers respond to therapy. A validation study using an independent cohort is also crucial to further reduce the risk of overfitting when testing multiple markers in a single cohort. (4) In this study, blood samples from Fujian Medical University were collected post-meals, whereas those from The First Affiliated Hospital,

Zhejiang University School of Medicine were obtained pre-meals, which may introduce variability associated with mealtime. Although the results obtained in AD and PD patients were largely replicated in two different cohorts, future investigations should eliminate differences in sample collection processes, particularly when involving samples from various geographically diverse hospitals. (5) Last but not least, although combining microglial markers with neuronal markers ($NMDAR2A^+$ and NFL^+ EVs) significantly improved differentiation power, the use of microglial EVs as a standalone tool is limited due to overlap with HC and HAM patients, i.e., further investigation is needed to identify better markers for better managing MS clinically.

Conclusions

In summary, this study introduced a novel biomarker for identifying microglial specific EVs in human blood through the dual labeling of CX3CR1 and UCHL1. We investigated the diagnostic and differential diagnostic potential of these $CX3CR1^+/UCHL1^+$ EVs in conjunction with $NMDAR2A^+$ and NFL^+ EVs for MS. Although further investigation is needed, our study offers a novel perspective on utilizing microglia-derived EVs in peripheral blood as a biomarker for the diagnosis and differential diagnosis of MS and related disorders.

Abbreviations

EVs	Extracellular vesicles
MS	Multiple sclerosis
HAM	HTLV-1 associated myelopathy
AD	Alzheimer's disease
PD	Parkinson's disease
CNS	Central nervous system
BBB	Blood-brain barrier
CSF-1	Colony-stimulating factor 1
qPCR	Quantitative real-Time-PCR
WB	Western blot
PFA	Paraformaldehyde
CSF	Cerebral spinal fluid
PVL	Proviral load
SEM	Standard error of mean
STORM	Ultra-high resolution imaging technique
TEM	Transmission electron microscope
NTA	Nano Tracking Analysis
Simoa	The Single Molecule Array
AUC	Area Under the Curve

Supplementary Information

The online version contains supplementary material available at https://doi.org/10.1186/s12974-024-03243-z.

Supplementary Material 1

Supplementary Material 2

Acknowledgements

We deeply appreciate the participants for their generous donation of samples.

Author contributions

JZ, YF, XB, JD, and CT conceptualized the study, JZ, YF, XB, JD, CT, and YY designed experiments. AWL, ZG, QL, JB, XTY, GPP, and BYL helped to collect the sample, JD and AWL carried out experiments. JD, ZG, and QL analyzed the data. JD wrote the manuscript, with guidance from JZ, YF, and XB. All authors read and approved the final manuscript.

Funding

This work was supported by: National Natural Science Foundation of China [grant numbers 82020108012, 82371250, and 82201560], Natural Science Foundation of Zhejiang Province [grant numbers LZ23H090002 and LY24H090006], Key R&D Program of Zhejiang [grant number 2024C03098], Leading Innovation and Entrepreneurship Team of Zhejiang Province [grant number 2020R01001], and Innovative Institute of Basic Medical Science of Zhejiang University. The funding body didn't play a role in the design of the study and collection, analysis, interpretation of data, or in writing the manuscript.

Data availability

No datasets were generated or analysed during the current study.

Declarations

Ethics approval and consent to participate

All procedures were performed in compliance with relevant laws and institutional guidelines and approved by the appropriate institutions (Clinical Research Ethics approval no.NCT04386018 from Fujian Medical University and no.2022-043 from The First Affiliated Hospital, Zhejiang University School of Medicine), and informed consent was obtained from each patient. The privacy rights of human subjects had always been observed.

Consent for publication

Not applicable.

Competing interests

The authors declare no competing interests.

Received: 6 June 2024 / Accepted: 23 September 2024
Published online: 09 October 2024

References

1. Gullotta GS, Costantino G, Sortino MA, Spampinato SF. Microglia and the Blood-Brain Barrier: An External Player in Acute and Chronic Neuroinflammatory Conditions. Int J Mol Sci. 2023; 24.
2. Walsh J, Tozer DJ, Sari H, Hong YT, Drazyk A, Williams G, et al. Microglial activation and blood-brain barrier permeability in cerebral small vessel disease. Brain. 2021; 144:1361–1371.
3. Candelario-Jalil E, Dijkhuizen RM, Magnus T. Neuroinflammation, Stroke, Blood-Brain Barrier Dysfunction, and Imaging Modalities. Stroke. 2022; 53:1473–1486.
4. Chang H, Ma J, Feng K, Feng N, Wang X, Sun J, et al. Elevated blood and cerebrospinal fluid biomarkers of microglial activation and blood–brain barrier disruption in anti-NMDA receptor encephalitis. J Neuroinflammation. 2023; 20:172.
5. Nishihara H, Perriot S, Gastfriend BD, Steinfort M, Cibien C, Soldati S, et al. Intrinsic blood-brain barrier dysfunction contributes to multiple sclerosis pathogenesis. Brain. 2022; 145:4334–4348.
6. Azodi S, Nair G, Enose-Akahata Y, Charlip E, Vellucci A, Cortese I, et al. Imaging spinal cord atrophy in progressive myelopathies: HTLV-I-associated neurological disease (HAM/TSP) and multiple sclerosis (MS). Ann Neurol. 2017; 82:719–728.
7. Leon SF, Arimura K, Osame M. Multiple sclerosis and HTLV-I associated myelopathy/tropical spastic paraparesis are two distinct clinical entities. Mult Scler. 1996; 2:88–90.
8. Zhao M, Jiang XF, Zhang HQ, Sun JH, Pei H, Ma LN, Cao Y, Li H. Interactions between glial cells and the blood-brain barrier and their role in Alzheimer's disease. Ageing Res Rev. 2021; 72:101483.

9. Sweeney MD, Sagare AP, Zlokovic BV. Blood-brain barrier breakdown in Alzheimer disease and other neurodegenerative disorders. Nat Rev Neurol. 2018; 14:133–150.
10. Xiang X, Wind K, Wiedemann T, Blume T, Shi Y, Briel N, et al. Microglial activation states drive glucose uptake and FDG-PET alterations in neurodegenerative diseases. Sci Transl Med. 2021; 13:eabe5640.
11. Biechele G, Blume T, Deussing M, Zott B, Shi Y, Xiang X, et al. Pre-therapeutic microglia activation and sex determine therapy effects of chronic immunomodulation. Theranostics. 2021; 11:8964–8976.
12. Dutta S, Hornung S, Taha HB, Bitan G. Biomarkers for parkinsonian disorders in CNS-originating EVs: promise and challenges. Acta Neuropathol. 2023; 145:515–540.
13. Tian C, Stewart T, Hong Z, Guo Z, Aro P, Soltys D, et al. Blood extracellular vesicles carrying synaptic function- and brain-related proteins as potential biomarkers for Alzheimer's disease. Alzheimer's & Dementia. 2022; 19:909–923.
14. Wang P, Lan G, Xu B, Yu Z, Tian C, Lei X, Meissner WG, Feng T, Yang Y, Zhang J. α-Synuclein-carrying astrocytic extracellular vesicles in Parkinson pathogenesis and diagnosis. Transl Neurodegener. 2023; 12:40.
15. Yu Z, Shi M, Stewart T, Fernagut PO, Huang Y, Tian C, et al. Reduced oligodendrocyte exosome secretion in multiple system atrophy involves SNARE dysfunction. Brain. 2020; 143:1780–1797.
16. Ginhoux F, Greter M, Leboeuf M, Nandi S, See P, Gokhan S, et al. Fate mapping analysis reveals that adult microglia derive from primitive macrophages. Science. 2010; 330:841–845.
17. Goldmann T, Wieghofer P, Müller PF, Wolf Y, Varol D, Yona S, et al. A new type of microglia gene targeting shows TAK1 to be pivotal in CNS autoimmune inflammation. Nat Neurosci. 2013; 16:1618–1626.
18. Salter Michael W, Beggs S. Sublime Microglia: Expanding Roles for the Guardians of the CNS. Cell. 2014; 158:15–24.
19. Schulz C, Gomez Perdiguero E, Chorro L, Szabo-Rogers H, Cagnard N, Kierdorf K, et al. A lineage of myeloid cells independent of Myb and hematopoietic stem cells. Science. 2012; 336:86–90.
20. Hashimoto D, Chow A, Noizat C, Teo P, Beasley MB, Leboeuf M, et al. Tissue-resident macrophages self-maintain locally throughout adult life with minimal contribution from circulating monocytes. Immunity. 2013; 38:792–804.
21. Yona S, Kim KW, Wolf Y, Mildner A, Varol D, Breker M, et al. Fate mapping reveals origins and dynamics of monocytes and tissue macrophages under homeostasis. Immunity. 2013; 38:79–91.
22. Shi M, Bradner J, Hancock AM, Chung KA, Quinn JF, Peskind ER, et al. Cerebrospinal fluid biomarkers for Parkinson disease diagnosis and progression. Ann Neurol. 2011; 69:570–580.
23. Mata IF, Shi M, Agarwal P, Chung KA, Edwards KL, Factor SA, et al. SNCA variant associated with Parkinson disease and plasma alpha-synuclein level. Arch Neurol. 2010; 67:1350–1356.
24. Shi M, Liu C, Cook TJ, Bullock KM, Zhao Y, Ginghina C, et al. Plasma exosomal α-synuclein is likely CNS-derived and increased in Parkinson's disease. Acta Neuropathol. 2014; 128:639–650.
25. Shi M, Kovac A, Korff A, Cook TJ, Ginghina C, Bullock KM, et al. CNS tau efflux via exosomes is likely increased in Parkinson's disease but not in Alzheimer's disease. Alzheimers Dement. 2016; 12:1125–1131.
26. Hong Z, Tian C, Stewart T, Aro P, Soltys D, Bercow M, et al. Development of a Sensitive Diagnostic Assay for Parkinson Disease Quantifying α-Synuclein-Containing Extracellular Vesicles. Neurology. 2021; 96:e2332-e2345.
27. Eberly LE. Multiple linear regression. Methods Mol Biol. 2007; 404:165–187.
28. Hu J, Szymczak S. A review on longitudinal data analysis with random forest. Brief Bioinform. 2023; 24.
29. Ji GJ, Hu P, Liu TT, Li Y, Chen X, Zhu C, Tian Y, Chen X, Wang K. Functional Connectivity of the Corticobasal Ganglia-Thalamocortical Network in Parkinson Disease: A Systematic Review and Meta-Analysis with Cross-Validation. Radiology. 2018; 287:973–982.
30. Yang J, Hamade M, Wu Q, Wang Q, Axtell R, Giri S, Mao-Draayer Y. Current and Future Biomarkers in Multiple Sclerosis. Int J Mol Sci. 2022; 23.
31. Disanto G, Barro C, Benkert P, Naegelin Y, Schädelin S, Giardiello A, et al. Serum Neurofilament light: A biomarker of neuronal damage in multiple sclerosis. Ann Neurol. 2017; 81:857–870.
32. Sumowski JF, Rocca MA, Leavitt VM, Meani A, Mesaros S, Drulovic J, Preziosa P, Habeck CG, Filippi M. Brain reserve against physical disability progression over 5 years in multiple sclerosis. Neurology. 2016; 86:2006–2009.
33. Li Q, Barres BA. Microglia and macrophages in brain homeostasis and disease. Nat Rev Immunol. 2018; 18:225–242.
34. Gomez Perdiguero E, Klapproth K, Schulz C, Busch K, Azzoni E, Crozet L, Garner H, Trouillet C, de Bruijn MF, Geissmann F, Rodewald HR. Tissue-resident macrophages originate from yolk-sac-derived erythro-myeloid progenitors. Nature. 2015; 518:547–551.
35. Mass E, Ballesteros I, Farlik M, Halbritter F, Günther P, Crozet L, et al. Specification of tissue-resident macrophages during organogenesis. Science. 2016; 353.
36. Brandenburg S, Blank A, Bungert AD, Vajkoczy P. Distinction of Microglia and Macrophages in Glioblastoma: Close Relatives, Different Tasks? Int J Mol Sci. 2020; 22.
37. Nishinakamura R, Takasato M. Essential roles of Sall1 in kidney development. Kidney Int. 2005; 68:1948–1950.
38. Su N, März S, Plagemann T, Cao J, Schnittler HJ, Eter N, Heiduschka P. Occurrence of Transmembrane Protein 119 in the Retina is Not Restricted to the Microglia: An Immunohistochemical Study. Transl Vis Sci Technol. 2019; 8:29.
39. Bassiouni M, Smorodchenko A, Olze H, Szczepek AJ. Identification and Characterization of TMEM119-Positive Cells in the Postnatal and Adult Murine Cochlea. Brain Sci. 2023; 13.
40. Su X, Floyd DH, Hughes A, Xiang J, Schneider JG, Uluckan O, et al. The ADP receptor P2RY12 regulates osteoclast function and pathologic bone remodeling. J Clin Invest. 2012; 122:3579–3592.
41. Liang Z, Damianou A, Vendrell I, Jenkins E, Lassen FH, Washer SJ, et al. Proximity proteomics reveals UCH-L1 as an essential regulator of NLRP3-mediated IL-1β production in human macrophages and microglia. Cell Rep. 2024; 43:114152.
42. Mi Z, Graham SH. Role of UCHL1 in the pathogenesis of neurodegenerative diseases and brain injury. Ageing Res Rev. 2023; 86:101856.
43. Hansen DV, Hanson JE, Sheng M. Microglia in Alzheimer's disease. J Cell Biol. 2018; 217:459–472.
44. Guo M, Wang J, Zhao Y, Feng Y, Han S, Dong Q, Cui M, Tieu K. Microglial exosomes facilitate α-synuclein transmission in Parkinson's disease. Brain. 2020; 143:1476–1497.
45. Isik S, Yeman Kiyak B, Akbayir R, Seyhali R, Arpaci T. Microglia Mediated Neuroinflammation in Parkinson's Disease. Cells. 2023; 12.
46. Yu H, Chang Q, Sun T, He X, Wen L, An J, Feng J, Zhao Y. Metabolic reprogramming and polarization of microglia in Parkinson's disease: Role of inflammasome and iron. Ageing Res Rev. 2023; 90:102032.
47. Leng F, Edison P. Neuroinflammation and microglial activation in Alzheimer disease: where do we go from here? Nat Rev Neurol. 2021; 17:157–172.
48. Tansey MG, Wallings RL, Houser MC, Herrick MK, Keating CE, Joers V. Inflammation and immune dysfunction in Parkinson disease. Nat Rev Immunol. 2022; 22:657–673.
49. Distéfano-Gagné F, Bitarafan S, Lacroix S, Gosselin D. Roles and regulation of microglia activity in multiple sclerosis: insights from animal models. Nat Rev Neurosci. 2023; 24:397–415.
50. Cignarella F, Filipello F, Bollman B, Cantoni C, Locca A, Mikesell R, et al. TREM2 activation on microglia promotes myelin debris clearance and remyelination in a model of multiple sclerosis. Acta Neuropathol. 2020; 140:513–534.
51. Prada I, Furlan R, Matteoli M, Verderio C. Classical and unconventional pathways of vesicular release in microglia. Glia. 2013; 61:1003–1017.
52. Abe M, Umehara F, Kubota R, Moritoyo T, Izumo S, Osame M. Activation of macrophages/microglia with the calcium-binding proteins MRP14 and MRP8 is related to the lesional activities in the spinal cord of HTLV-I associated myelopathy. J Neurol. 1999; 246:358–364.
53. Höllsberg P. Pathogenesis of chronic progressive myelopathy associated with human T-cell lymphotropic virus type I. Acta Neurol Scand Suppl. 1997; 169:86–93.
54. Afonso PV, Ozden S, Cumont MC, Seilhean D, Cartier L, Rezaie P, et al. Alteration of blood-brain barrier integrity by retroviral infection. PLoS Pathog. 2008; 4:e1000205.
55. Nozuma S, Jacobson S. Neuroimmunology of Human T-Lymphotropic Virus Type 1-Associated Myelopathy/Tropical Spastic Paraparesis. Front Microbiol. 2019; 10:885.
56. Brunetto GS, Massoud R, Leibovitch EC, Caruso B, Johnson K, Ohayon J, Fenton K, Cortese I, Jacobson S. Digital droplet PCR (ddPCR) for the precise quantification of human T-lymphotropic virus 1 proviral loads in peripheral blood and cerebrospinal fluid of HAM/TSP patients and identification of viral mutations. J Neurovirol. 2014; 20:341–351.
57. Faissner S, Plemel JR, Gold R, Yong VW. Progressive multiple sclerosis: from pathophysiology to therapeutic strategies. Nat Rev Drug Discov. 2019; 18:905–922.
58. Novakova L, Axelsson M, Malmeström C, Zetterberg H, Blennow K, Svenningsson A, Lycke J. NFL and CXCL13 may reveal disease activity in clinically and radiologically stable MS. Mult Scler Relat Disord. 2020; 46:102463.

59. Barro C, Leocani L, Leppert D, Comi G, Kappos L, Kuhle J. Fluid biomarker and electrophysiological outcome measures for progressive MS trials. Mult Scler. 2017; 23:1600–1613.
60. Singh J, Habean ML, Panicker N. Inflammasome assembly in neurodegenerative diseases. Trends Neurosci. 2023; 46:814–831.
61. Carotenuto A, Signoriello E, Lanzillo R, Vaia Y, Moccia M, Bonavita S, Lus G, Brescia Morra V. Unraveling diagnostic uncertainty in transition phase from relapsing-remitting to secondary progressive multiple sclerosis. Mult Scler Relat Disord. 2020; 43:102211.
62. Ziemssen T, Bhan V, Chataway J, Chitnis T, Campbell Cree BA, Havrdova EK, et al. Secondary Progressive Multiple Sclerosis: A Review of Clinical Characteristics, Definition, Prognostic Tools, and Disease-Modifying Therapies. Neurol Neuroimmunol Neuroinflamm. 2023; 10.

Publisher's note